THE ASTROPHYSICAL JOURNAL, 454:580–592, 1995 December 1

POWERFUL EXTENDED RADIO SOURCES AS TOOLS TO ESTIMATE AMBIENT GAS DENSITIES, JET LUMINOSITIES, AND OTHER KEY PHYSICAL PARAMETERS

RUTH A. DALY[1]
Department of Physics, Joseph Henry Laboratories, Princeton University, Princeton, NJ 08544
Received 1994 September 27; accepted 1995 June 12

ABSTRACT

It would be quite valuable if the radio properties of powerful, extended radio sources could be used to deduce key physical quantities such as the density of the ambient gas in the vicinity of a radio source. It is shown here that radio observations can be used to estimate the ambient gas density, the luminosity in directed kinetic energy, and other key physical parameters relevant to the radio source and its gaseous environment. The methods described are applied to radio galaxies and radio-loud quasars with redshifts from about 0 to 2.

The ambient gas density in the vicinity of the radio lobes is estimated by applying the strong shock jump conditions across the forward edge of the radio bridge (referred to as the radio lobe); this requires that the lobe pressure and the lobe propagation velocity be known. The lobe pressure is estimated assuming minimum energy conditions, and the local propagation velocity is estimated from the effects of synchrotron and inverse Compton aging of relativistic electrons on the radio spectrum across the radio bridge. At present this appears to be the only method of estimating the ambient gas density (as a single parameter) in the vicinity of distant powerful radio sources, and this first application of the method indicates that it provides a good rough estimate of the ambient gas density.

One interesting result is that galaxies and quasars are found to lie in similar gaseous environments. Another is that the composite density profile is similar to that of gas in clusters of galaxies and is normalized to Cygnus A, which is known to be in a cluster with a hot intracluster medium in place. This suggests that the powerful radio sources considered here are surrounded by extended gaseous halos like those in present-day galaxy clusters, with the radio source interior to the core of the gaseous halo. One interpretation is that the radio sources considered are in the cores of clusters of galaxies with their intracluster media in place, which would suggest that some clusters, or at least cluster cores, exist out to redshifts of about 2.

The lobe propagation velocity, the rate at which energy is channeled from the central engine in the form of a collimated outflow (known as the luminosity in directed kinetic energy), and a time-independent characteristic source size, which provides a calibrated yardstick and hence is a useful cosmological tool, are also discussed. The basic assumptions adopted by Daly (1994) in the use of these sources as cosmological probes are empirically tested; it is found that the data are consistent with the assumptions adopted. Relations between different parameters are investigated and discussed in detail. This leads to a wide perspective and good understanding of the environments and nuclear properties of powerful extended radio sources. For example, a maximum value for the energy extraction rate is seen in the present data set and may imply an upper limit to this quantity. And the lobe propagation velocity may also have a maximum value, indicating that there may be an upper limit to the Mach number at which the radio lobe propagates into the ambient medium.

The limited data set used here supports the idea that radio galaxies and radio-loud quasars are intrinsically similar but appear different due to different viewing angles, however, they may not be intrinsically identical. Perhaps the two types of active galactic nucleus (AGN) activity observed, highly collimated outflows and radiant energy from the nuclear region of the AGN, should be identified with the two ultimate energy sources associated with massive compact objects: the spin energy of the massive compact object and the gravitational energy of matter falling onto the object, respectively. Then, the three types of AGN observed may not be intrinsically identical: radio-quiet quasars result when only the gravitational energy is being tapped, radio-loud quasars result when both energy sources are being tapped, and radio galaxies result when the spin energy of the massive compact object is being tapped. Since the sources are likely to be anisotropic, such a scheme is likely to be working in parallel with orientation unified models.

Subject headings: cosmology: theory — galaxies: jets — intergalactic medium — radio continuum: galaxies

1. INTRODUCTION

Powerful extended radio sources are observed over a broad range of redshift and out to fairly large redshift. These sources provide a means of probing the gaseous environments of extended radio sources, the intrinsic properties of the sources, and the evolution of their environments and properties. Extracting this information from the radio properties of the sources requires a detailed understanding of the interplay between intrinsic source properties and properties extrinsic to the source, such as the ambient gas density, that determine the time evolution of a given radio source.

A model for the time evolution of a powerful extended radio source, written in terms of fundamental physical variables that are simply related to observed quantities, is described by Daly (1990, 1994). This model is based upon the standard "beam

[1] National Young Investigator.

model" for radio sources developed and discussed by Blandford & Rees (1974), Scheuer (1974, 1982), De Young & Axford (1967), De Young (1971, 1986, 1991), Norman et al. (1982) Begelman, Blandford, & Rees (1984), Myers & Spangler (1985), Alexander & Leahy (1987, hereafter AL87), Prestage & Peacock (1988), Cox, Gull, & Scheuer (1991), Rawlings & Saunders (1991), Loken et al. (1992), and many others.

Extended radio sources with radio lobes that straddle the host galaxy are presumed to be powered by a central AGN. A collimate beam of particles and/or fields carries energy away from the AGN. The energy from the beam is deposited in the vicinity of the radio hot spot and lobe, causing a strong shock front to propagate into the medium. Electrons are accelerated to relativistic energies behind the forward shock front, near the contact discontinuity. The relativistic electrons left behind as the shock front propagates forward produce the observed radio emission via synchrotron radiation. The radio emission is observed from the radio hot spots and lobes, and the radio bridge that connects the lobe region with the central AGN (e.g., Leahy, Muxlow, & Stephens 1989; hereafter LMS89); the forward part of the radio bridge that comprises the roughly spherical region about the radio hot spot is referred to as the radio lobe.

Both the propagation of the radio hot spot and the propagation of the radio lobe are discussed in the literature. The propagation of the radio lobe is discussed here. The propagation of the radio lobe may be considered to be the temporal and spatial average of the propagation of the radio hot spot (Scheuer 1982; Begelman & Cioffi 1989; Daly 1990, 1994; Cox, Gull, & Scheuer 1991). As discussed below, the strong shock jump conditions are satisfied across the forward region of the radio lobe when the radio lobe propagates with a velocity which is large compared to the sound speed of the ambient medium. Thus, the propagation of the radio hot spot and the propagation of the radio lobe may be considered separately, as discussed explicitly by Cox, Gull, & Scheuer (1991), who confirm numerically that the strong shock jump conditions are satisfied across the lobe-medium interface. In particular, the radio lobe is ram pressure confined by the ambient medium so that $n_a v_L^2 \propto P_L$, where n_a is the ambient gas density, v_L is the lobe propagation velocity, and P_L is the lobe pressure.

Empirically, the position and properties of radio hot spots appear to vary on short timescales, while those of radio lobes tend to be much more stable (Black et al. 1992). The radio lobes of powerful extended radio sources most likely propagate supersonically. This is suggested both by their radio morphology (Prestage & Peacock 1988), and by the lobe propagation velocities as estimated from synchrotron and inverse Compton aging of relativistic electrons across the radio bridge, which yield velocities that are typically $\gtrsim 10^4$ km s^{-1} for 178 MHz radio powers greater than a few $h^{-2} \times 10^{26}$ W Hz^{-1} sr^{-1} estimated assuming $q_0 = 0$ (see AL87 and Table 1).

The velocity of propagation of the radio hot spot v_h depends on the rate of energy input to the hot spot L_j (known as the luminosity in directed kinetic energy), the cross-sectional area of the hot spot A_h, and the pressure of the hot spot p_h. The strong shock jump conditions imply that the hot spot pressure can be written in terms of the (preshock) ambient gas density n_a and the hot spot propagation velocity v_h: $p_h \propto n_a v_h^2$. The balance of momentum flux across the hot spot implies that $L_j/(v_j A_h) \propto n_a v_h^2$ (e.g., Blandford & Rees 1974; Scheuer 1974; Bridle & Perley 1984; Begelman, Blandford, & Rees 1984). Unfortunately, this expression cannot be applied to estimate L_j using radio data since several quantities in the expression cannot be deduced for most sources. However, as shown below (see eqs. [1] and [3]), it is possible to derive another expression for the rate of energy input L_j, or luminosity in directed kinetic energy, which can be simply related to observationally accessible quantities.

It is straightforward to show that the relation between the lobe propagation velocity v_L, the luminosity in directed kinetic energy L_j, the ambient gas density in the vicinity of the radio lobe n_a, and the cross-sectional radius of the radio lobe a_L is

$$L_j \propto n_a a_L^2 v_L^3 \quad (1)$$

(e.g., Daly 1990, 1994; Rawlings & Saunders 1991; Loken et al. 1992). The derivation discussed by Daly (1990, 1994) parallels

TABLE 1

PROPERTIES OF THE RADIO SOURCES

Source	Type	z	Size (h^{-1} kpc)	R_T	a_L (h^{-1} kpc)	B (10^{-5} G)	v_L ($10^{-2}c$)	n_a (10^{-3} cm^{-3})
3C 55	G	0.72	342	15.4	11	2.7	8.2	0.5
3C 68.1	Q	1.238	302	8.9	17	2.5	4.2	1.7
3C 68.2	GL	1.575	138	7.8*	8.8	5.1	7.5	2.2
3C 154.....	Q	0.580	218	5.4	20	1.1	1.2	3.9
3C 175.....	Q	0.768	237	5.9	20	1.8	2.1	3.3
3C 249.1.....	QL*	0.311	134	4.5	15	1.2	1.3	3.8
3C 263.....	Q	0.656	204	3.6	28	1.8	1.6	6.2
3C 265.....	G	0.811	394	11.7	17	2.0	4.2	1.0
3C 267.....	GL	1.144	216	9.2*	12	3.1	3.8	3.1
3C 268.1.....	GL	0.974	248	9.8*	13	3.2	5.5	1.6
3C 322.....	GL	1.681	207	8.5*	12	3.7	5.8	1.9
3C 330.....	GL	0.549	263	14.7*	8.9	2.4	4.0	1.6
3C 334.....	QL*	0.555	247	3.8	33	1.2	2.4	1.1
3C 356.....	G	1.079	419	13.9	15	1.6	3.3	1.1
3C 405.....	G	0.056	96	7.6	6.3	6.6	5.0	8.1
3C 427.1.....	G	0.572	100	7.7	6.5	4.9	4.1	6.8

NOTE.—The quantities listed in Table 1 are derived assuming $H_0 = 100$ km s^{-1} Mpc^{-1} and $q_0 = 0$. Galaxies are denoted by G, and galaxies with a lower bound on their axial ratio are denoted by GL; quasars are denoted by Q, and quasars with radio powers between $h^{-2}(10^{26}$–$10^{27})$ W Hz^{-1} sr^{-1} are denoted by QL*. An asterisk in col. (5) indicated that the axial ratio listed is a lower bound.

the derivations used by Parker (1963), McKee & Ostriker (1977), Chevalier & Imamura (1983), and Hundhausen (1985) to study shocks in other astrophysical settings.

It is easy to show that equation (1) is completely consistent with the more familiar equation balancing momentum flux across the hot spot. For example, models A and B proposed by Scheuer (1974) satisfy both equations simultaneously. As shown by Rawlings & Saunders (1991), equation (1) is valid whenever two very simple proportionalities hold: when the lobe-lobe separation is $D \propto v_L t$ and the total energy in the bridge is $E \propto L_j t$, as is the case for Scheuer's models A and B (see Scheuer 1974, eqs. [4], [8], [29], and [30]). Equation (1) follows since, for powerful extended radio sources, the bridge pressure is roughly constant and the volume V is roughly cylindrical, with $V \propto a_L^2 D$, where a_L is the radius and D the length of the cylinder (LMS89; Wellman & Daly 1995, 1996).

In order to be able to use equation (1) to estimate the luminosity in directed kinetic energy L_j, an estimate of the ambient gas density n_a is required. Generally, it is very difficult to obtain a direct estimate of the ambient gas density in the vicinity of the radio lobe. One exception is the nearby source Cygnus A (3C 405) that is located in a cluster of galaxies at a redshift of 0.056. The cluster is close enough that thermal bremsstrahlung X-ray emission from the intracluster gas is well resolved, and the X-ray surface brightness in the vicinity of the radio lobes can be used to estimate the ambient gas density near each lobe; this gas density is about 8×10^{-3} cm^{-3} for a Hubble constant of $H_0 = 100$ km s^{-1} Mpc^{-1} (Arnaud et al. 1984).

It is very unlikely that it will be possible to estimate the ambient gas density in the vicinity of the radio lobes of distant extended radio sources using X-ray data for several reasons. First, the X-ray emission is generally unresolved, so the observations only indicate a total X-ray luminosity for the cluster. Second, the AGN may be an X-ray source, and, third, the region of extended radio emission may be an X-ray source. All of these problems are exacerbated for sources at high redshift.

The ambient gas density in the vicinity of the radio lobes may be estimated using the strong shock jump conditions, which are nearly equivalent to the equation of ram pressure confinement $n_a v_L^2 \simeq p_L$, where p_L is the total pressure of the radio lobe. If rough pressure equilibrium between the magnetic and relativistic electron components within the lobe is assumed, the magnetic field strength B_L that minimizes the total energy provides a good rough approximation of the true field strength, and the total lobe pressure satisfies $p_L \propto B_L^2$. This implies that

$$n_a \propto \left(\frac{B_L}{v_L}\right)^2 . \tag{2}$$

The lobe propagation velocity can be estimated from the effects of synchrotron and inverse Compton aging of the relativistic electron population on the radio spectrum across the radio bridge and lobe (Myers & Spangler 1985; AL87; LMS89; Liu, Pooley, & Riley 1992; hereafter LPR92). This has been studied in detail for the case of Cygnus A for which there is extensive high-resolution data (Carilli et al. 1991), and, though some details are not yet understood, the model appears to yield a good order of magnitude estimate of the lobe propagation velocity.

The luminosity in directed kinetic energy can be estimated by combining equations (1) and (2):

$$L_j \propto v_L a_L^2 B^2 . \tag{3}$$

Thus, the luminosity in directed kinetic energy can be estimated from radio observations and is discussed in detail in § 2.2.

The ways that the radio observations may be used to estimate the quantities on the right-hand sides of equations (2) and (3), and thus to estimate the density of the ambient medium and the luminosity in directed kinetic energy for radio galaxies and radio-loud quasars, are demonstrated in § 2. The environments and nuclear properties of sources, the evolution of the environments and source properties, and the relations between various parameters are discussed in this section. The assumptions adopted by Daly (1994) in developing a model in which extended radio sources can be used as a calibrated yardstick, and thus as a cosmological tool, are shown to be consistent with the data. Characteristic source sizes that may provide a calibrated yardstick are discussed in § 2.4. The implications of these observations for "orientation unified models" and for other ways of viewing the different types of AGN are discussed in § 3. Values of the Hubble constant of $H_0 = 100\ h$ km s^{-1} Mpc^{-1} and the deceleration parameter $q_0 = 0$ are assumed throughout unless otherwise noted.

2. APPLICATION TO ESTIMATE KEY PHYSICAL PARAMETERS

Equations (1), (2), and (3) are valid when the lobe propagation velocity is large compared with the sound speed of the ambient gas, so the lobe propagates supersonically. The velocity estimated from the synchrotron and inverse Compton aging of relativistic electrons is a good approximation to the lobe propagation velocity when backflows are negligible. As discussed by Leahy & Williams (1984) and Daly (1994), this is likely to be the case when the 178 MHz radio power is greater than about $h^{-2} \times (10^{26}$ to $10^{27})$ W Hz^{-1} sr^{-1}.

The data presented by LMS89 are used here. All of the radio galaxies and most of the quasars in the LMS89 sample have 178 MHz radio powers greater than $h^{-2} \times 10^{27}$ W Hz^{-1} sr^{-1}; two of the radio-loud quasars have radio powers in the range from $(10^{26}$ to $10^{27})$ W Hz^{-1} sr^{-1}. It is interesting to note that this range of radio powers is similar to that at which the sources become supersonic, having lobe propagation velocities $\gtrsim 10^{-2} c$ (AL87), where c is the speed of light.

The LMS89 data have been used to estimate the ambient gas density n_a (§ 2.1), the luminosity in directed kinetic energy L_j (§ 2.2), the lobe propagation velocity v_L (§ 2.3 and Table 1), the characteristic sources sizes l_* (§ 2.4), and several other observables such as the opening angle of the bridge, the lobe radii, and the lobe axial ratios (§ 2.5).

In all figures, radio galaxies are represented as filled symbols, and radio-loud quasars as open symbols and crosses. The axial ratio of a radio source is a measure of the ratio of the source length to the width (Leahy & Williams 1984; LMS89). All of the radio-loud quasars have resolved axial ratios. Radio-loud quasars with 178 MHz radio powers above $h^{-2} \times 10^{27}$ W Hz^{-1} sr^{-1} are represented as open circles, while the two sources with radio powers in the range from $h^{-2} \times (10^{26}$ to $10^{27})$ W Hz^{-1} sr^{-1} are represented as crosses. Radio galaxies are represented by filled squares if the quantity plotted does not explicitly depend on the axial ratio of the source, or if the axial ratio of the source is resolved. Radio galaxies are represented as filled triangles when the quantity plotted depends on the axial ratio and the axial ratio of the source is unresolved; the direction of the arrow indicates whether the quantity is bounded from above or below. One radio-loud quasar, 3C 68.1 at a redshift of 1.2, sits with the radio galaxies on

essentially all of the figures and may represent a transition case between radio-loud quasars and radio galaxies, or it may be a radio galaxy rather than a radio-loud quasar.

The error bars shown on the figures have been estimated assuming zero uncertainty for the lobe-lobe separation, a 20% uncertainty for the axial ratio, the lobe radius, and the break frequency (LMS89), a magnetic field strength proportional to the depth of the source to the $-\frac{2}{7}$ power, and a 10% uncertainty for the fraction f_D of the lobe-lobe separation over which radio emission is detected and used by LMS89 to estimate the synchrotron age of the source; f_D is necessary to estimate the velocity (see § 2.3) and was measured using a ruler. These uncertainties imply about a 30% uncertainty for the ambient gas density, a 25% uncertainty for the luminosity in directed kinetic energy, a 15% to 20% uncertainty for the velocity of lobe propagation, a 15% to 20% uncertainty for the parameter k that is related to the characteristic source size l_*, a 20% uncertainty for l_* assuming $\beta = 1.5$ (see § 2.4) and a 20% uncertainty for the tangent of the half-opening angle θ.

If the magnetic field strength is taken to be proportional to the depth of the source to the $-\frac{4}{7}$ power, then the implied uncertainties are all about the same, except that for the luminosity in directed kinetic energy, which is decreased to about 14%. This affects the figures discussed in § 2.2 in the sense that the reduced χ^2 all increase by about a factor of 3.

The error bars used here are only approximate for the following reasons. All of quantities mentioned above, except for the half-opening angle θ, depend on the velocity of lobe propagation, and hence on the age of the source. The uncertainties noted above are estimated assuming that synchrotron cooling is much more important than inverse Compton cooling with microwave background photons, that is, it is assumed that the energy density of the magnetic field is much greater than that of the microwave background radiation at the redshift of the source. However, this is not a good approximation for some of the sources considered. Further, the field may be less than the minimum energy field, as suggested by Carilli et al. (1991) for the case of Cygnus A (see the discussion in § 2.1). A reanalysis of the LMS89 data and of the LPR92 data has been carried out by Wellman & Daly (1995, 1996) and results similar to those presented here are obtained. A discussion of the errors for the cases in which the energy density of the magnetic field is comparable to, or less than, that of the microwave background radiation at the redshift of the source, is included in Wellman & Daly (1995, 1996), who also consider the possibility that the magnetic field is typically a factor of about 3 less than the minimum energy value.

Several source properties are listed in Table 1. The source name is given in column (1), whether the source is classified as a galaxy (G) or quasar (Q) is given in column (2); GL indicates that the axial ratio of the galaxies is a lower bound, and this is also indicated in column (5) by an asterisk; QL* implies that the quasar falls within the 178 MHz radio power range from $h^{-2} \times (10^{26}$ to $10^{27})$ W Hz^{-1} sr^{-1}. The source redshift, lobe-lobe size, axial ratio, and the minimum energy magnetic field as estimated by LMS89 are listed in columns (3), (4), (5), and (7). Quantities estimated or inferred from those listed in LMS89 are listed in columns (6), (8), and (9), and, are respectively, the lobe radius or bridge width estimated from the lobe-lobe size and the axial ratio (see § 2.5), the velocity of lobe propagation estimated from the size and synchrotron age of the source (see § 2.3), and the ambient gas density estimated using equation (2).

The relations between various quantities are investigated and the slope, m, and y intercept, b, of the best-fit line given by $y = mx + b$, to the data are listed in Table 2. The data and best-fit lines are illustrated in the figure indicated in column (1); if the figure is not shown, "ns" is entered in column (1). In

TABLE 2

BEST-FIT PARAMETERS

Figure	Type	y	x	m	b	Reduced χ^2
1*a*.....	G+Q	log n_a	log (1 + z)	−1.4 ± 0.3	−2.4 ± 0.1	6.7
1*b*.....	G+Q	log n_a	log D(kpc)	−1.4 ± 0.2	0.6 ± 0.4	2.9
1*c*.....	G+Q	log n_a(96)	log (1 + z)	−0.3 ± 0.3	−2.1 ± 0.1	2.8
2*a*.....	G+Q	log L_j	log D (kpc)	−0.1 ± 0.1	47. ± 0.3	19.
2*a*.....	G	log L_j	log D (kpc)	−0.6 ± 0.2	48. ± 0.4	8.1
2*b*.....	G	log L_j	log (1 + z)	0.7 ± 0.3	46. ± 0.1	9.1
2*c*.....	G	log L_j	log (P_r)	0.7 ± 0.1	27. ± 3.	5.1
ns.....	G+Q	log L_j	log ($P_r\sqrt{\nu_b}$)	0.8 ± 0.1	25. ± 2.	7.1
2*d*.....	G+Q	log L_j	log (v_L/c)	1.4 ± 0.1	49. ± 0.2	5.9
2*d*.....	G	log L_j	log (v_L/c)	1.9 ± 0.3	49. ± 0.3	3.8
2*e*.....	G	log ($n_a a_L^2$)	log (v_L/c)	−1.1 ± 0.6	−0.7 ± 0.7	0.8
2*e*.....	G+Q	log ($n_a a_L^2$)	log (v_L/c)	−1.6 ± 0.2	−1.2 ± 0.3	1.2
ns.....	G	log (v_L/c)	log ($n_a a_L^2$)	−0.3 ± 0.1	−1.0 ± 0.1	2.2
ns.....	G+Q	log (v_L/c)	log ($n_a a_L^2$)	−0.5 ± 0.05	−1.0 ± 0.05	3.4
3*a*.....	G	log (v_L/c)	log (1 + z)	0.2 ± 0.2	−1.3 ± 0.1	3.4
3*b*.....	G	log (v_L/c)	log D(kpc)	−0.1 ± 0.1	−1. ± 0.3	3.4
3*c*.....	G+Q	log (v_L/c)	log (P_r)	0.4 ± 0.04	−12. ± 1.2	6.2
3*c*.....	G	log (v_L/c)	log (P_r)	0.2 ± 0.1	−6.0 ± 2.4	3.0
4*a*.....	G	k	z	−0.004 ± 0.07	0.6 ± 0.1	1.0
4*b*.....	G	k	D	0.0002 ± 0.0003	0.5 ± 0.1	0.9
4*c*.....	G	$l_*(\beta = 1.5)$	z	−0.1 ± 0.2	1.9 ± 0.2	1.1
4*d*.....	G	$l_*(\beta = 1.5)$	D	0.0015 ± 0.001	1.5 ± 0.3	0.9
4*e*.....	G	log [l_*(1.5)]	log (1 + z)	−0.1 ± 0.3	0.3 ± 0.1	1.3
4*f*.....	G	log [l_*(3.0)]	log (1 + z)	−0.5 ± 0.3	1.9 ± 0.1	3.5
5*a*.....	G	θ	z	1.0 ± 0.9	4.2 ± 0.8	2.0
5*b*.....	G	a_L	z	3.3 ± 1.2	6.6 ± 1.0	1.9
ns.....	G	R_T	z	−0.1 ± 1.1	9.4 ± 1.2	1.8

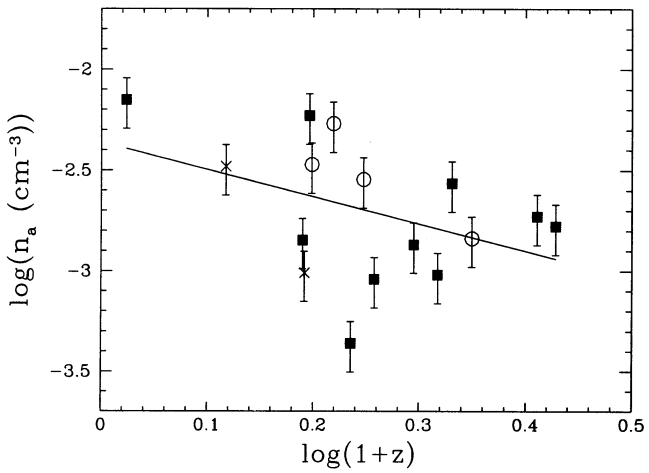

FIG. 1a

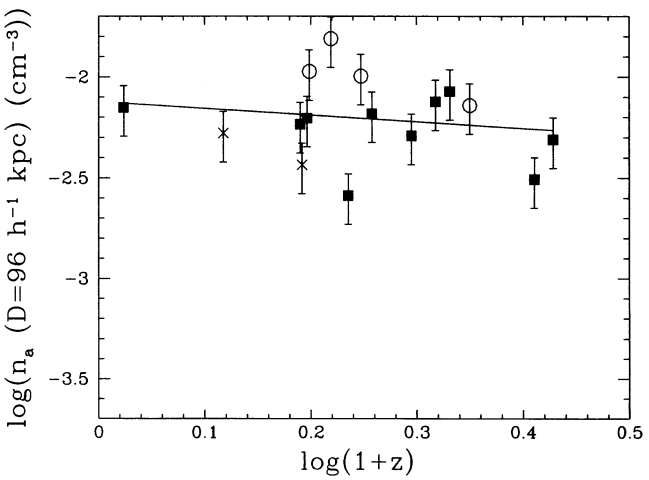

FIG. 1c

FIG. 1.—(*a–c*) Radio galaxies are denoted by filled squares. Quasars with 178 MHz powers between $h^{-2} \times (10^{26}$ and $10^{27})$ W Hz^{-1} sr^{-1} are denoted by crosses, while quasars with powers greater than $h^{-2} \times 10^{27}$ W Hz^{-1} sr^{-1} are denoted by open circles. Parameters of the best fitting lines are given in Table 2.

some fits, both galaxies and quasars are included, and in others, only galaxies are included as indicated in column (2). The reduced χ^2 of each fit is listed in column (7).

2.1. *Ambient Gas Density*

A key physical quantity is the density of the ambient gas in the vicinity of the radio lobe. If a method could be developed to estimate this quantity, it would be quite valuable since at the present time there are only indirect ways to estimate the gas content, such as rotation measure studies. The ambient gas density is important not only for the effect on the rate of growth of the radio source, but also because it provides a probe of evolution of structure in the universe. For example, the data discussed here suggest that clusters of galaxies, or at least cluster cores, with their intracluster medium in place, exist out to redshifts of about 2. This is expected in models of structure formation and evolution in which structure formation is well under way at early epochs, as is expected in a low-density cosmological model.

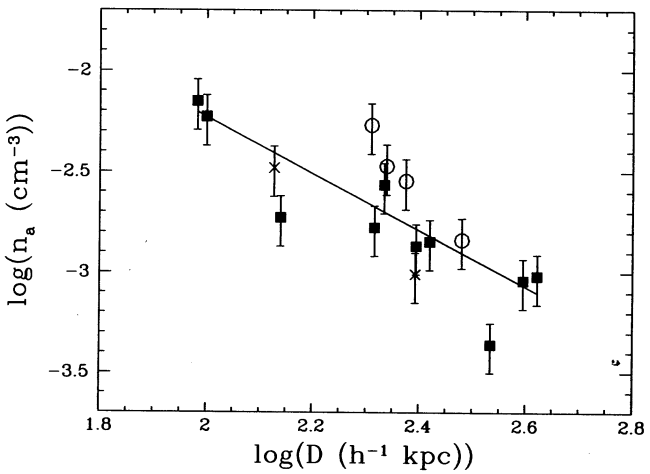

FIG. 1b

Equation (2) has been used to estimate the ambient gas density in the vicinity of the radio lobes for the radio sources discussed by LMS89. The ambient gas density estimated in this way is independent of the axial ratio of the source and thus can be estimated for all of the sources. The lobe propagation velocity is deduced from the data as described in § 2.3. The density is normalized to Cygnus A, which is inferred to have a density of about 8×10^{-3} cm^{-3} in the vicinity of the radio lobes assuming a value of $h = 1.0$ (Arnaud et al. 1984).

The ambient gas density is plotted as a function redshift on Figure 1*a*. There is no tendency for the ambient gas density to increase with redshift; if anything, a slight decrease with redshift is indicated: $n_a \propto (1 + z)^{-1}$. The facts that the ambient gas density evolves weakly with redshift and that the range of density spans about an order of magnitude indicate that the sources are in fairly similar environments.

It is interesting to note that the galaxies and quasars seem to inhabit similar environments, which is also evident in the other figures. This suggests that it may be necessary for a source to be in gas-rich environment to become a very powerful radio emitter.

The ambient gas density is plotted as a function of radio lobe separation to obtain a composite density profile, which is shown in Figure 1*b*. It turns out that the radio lobes of the sources considered are fairly symmetric about the estimated position of the AGN, so the AGN-lobe distance r is about half of the lobe-lobe separation D. The composite profile follows $n_a \propto r^{-1.4}$, where r is the distance from the center of the source. The slope is measured over a factor of 4 in distance, for distances measured from the core of the AGN of 100–400 kpc for $h = 0.5$. This slope is similar to that of gas in low-redshift clusters of galaxies at these distances from the cluster center (Jones & Forman 1984) and has a normalization similar to that of gas in low-redshift clusters by definition since it is normalized to Cygnus A. The reduced χ^2 of about 3 indicates that the ambient gas density can be estimated to about 50% accuracy rather than the 30% accuracy allowed by observational uncertainties. This suggests that the combined errors due to both the real scatter of the environments of the sources and deviations from the minimum energy conditions are quite small, about 40%. Thus, if the radio lobes of Cygnus A deviate from minimum energy conditions as suggested by Carilli et al. (1991), the other radio sources probably deviate in a similar manner.

As pointed out by L. Rudnick (1994, private communication), this slope may be an input rather than an output. This is possible since the velocity estimate involves $v_L \propto D$ (see § 2.3). However, if this were the origin of the relation $n_a \propto D^{-1.4}$, we would expect a relation between v_L and D, of the order $v_L \propto D$. Figure 3*c* shows that v_L is essentially independent of D, as discussed in § 2.3. The magnetic field strength B is also independent of D. Thus, the relation indicated using equation (2), $n_a \propto r^{-1.4}$, is an output rather than an input.

Much of the scatter seen in Figure 1*a* is due to the fact that the ambient gas density around different sources is estimated at different distances $r \sim D/2$ from the radio galaxy or cluster core. The density at a fixed position $D = 96\,h^{-1}$ kpc, chosen to coincide with the lobe-lobe separation of Cygnus A, can be estimated assuming the density profile about a given source is the same as the composite density profile. This normalized density is shown as a function of redshift in Figure 1*c*.

The trend shown in Figure 1*c* indicates that any evolution of the gaseous environments of the radio sources with redshift is rather weak, and that much of the scatter seen in Figure 1*a* arises because the gas density is measured at different distances from the center of the source. The reduced χ^2 of the fit is about 3, similar to that shown in Figure 1*b*. As with the reduced χ^2 of Figure 1*b*, this suggests that there is about a 40% scatter due to real differences of the gaseous environments of the sources, and/or rather modest scatter introduced by deviations from the conditions in the lobes of Cygnus A. The reduced χ^2 for Figures 1*b* and 1*c* suggest that equation (2) can be used to estimate ambient gas densities to about 50% accuracy, a tentative yet remarkable result.

Figures 1*b* and 1*c* suggest that radio galaxies and radio-loud quasars are in similar gaseous environments; the radio sources are in gaseous environments like the intracluster media in present-day clusters of galaxies (at least out to radii from the cluster center of about 200 h^{-1} kpc); the radio sources are located near the base of the gravitational potential well; and, if the sources are in clusters of galaxies, then the properties of the intracluster media evolve weakly, if at all, with redshift. This may indicate that it is necessary for a source to be in a rather gas-rich environment for the jet-medium interaction to produce a very powerful radio emitter.

The fact that equation (2) can be used to estimate the ambient gas density suggests that the velocity of lobe propagation estimated from synchrotron and inverse Compton aging is at least proportional to the lobe propagation velocity, and that the minimum energy magnetic fields in the bridges of radio sources, which was used to approximate the pressure of the radio-emitting plasma in the lobe, is at least proportional to the square root of the lobe pressure.

It is curious to note that, for the case of Cygnus A and thus for all of the sources considered here, the application of the equation of ram pressure confinement $\rho_a v_L^2 \simeq p_L$ implies that the energy density of the plasma in the lobe is about 100 times larger than estimated assuming minimum energy conditions and a lobe field strength similar to that in the bridge. As discussed by Carilli et al. (1991) for the case of Cygnus A, this discrepancy may be accounted for if the magnetic field strength is about a factor of 3 less than the equipartition value.

2.2. *Luminosity in Directed Kinetic Energy*

The rate at which energy is input to the hot spot and lobe may be estimated using equation (3). The luminosity in directed kinetic energy L_j can be normalized using Cygnus A, since for this source, independent estimates of the lobe radius a_L, the lobe propagation velocity v_L, and the mass density of the gas in the vicinity of the radio lobe ρ_a, exist. The strong shock jump conditions applied to the radio lobe imply that $L_j \sim \pi a_L^2 \rho_a v_L^3$ (e.g., § 3.1 of Daly 1994). Note that the normalization is $\propto v_L^3$ and thus is very sensitive to the absolute value of the lobe propagation velocity. The normalization here is obtained assuming $(v_L/c) \simeq 0.05$, which is the value of the lobe propagation velocity estimated using the method described in § 2.3. This value is consistent with that obtained by Carilli et al. (1991) using very detailed high-resolution radio data, since a value of $h = 1$ is assumed here compared with the value $h = 0.75$ assumed by Carilli et al. (1991), and the lobe propagation velocity scales as $h^{-4/7}$. As Carilli et al. (1991) note, the magnetic field strength may be less than the minimum energy value by about a factor of 3, indicating a lobe propagation velocity of about $0.01c$ since the lobe propagation velocity is proportional to $B^{1.5}$. This would change the normalization of L_j by a factor of about 125! Thus, the relative values of L_j are far more well determined than the absolute values.

The luminosity in directed kinetic energy is plotted as a function of lobe-lobe separation in Figure 2*a*; both galaxies and quasars are included in the fit that leads to the line with zero slope (see Table 2), and only galaxies are included in the fit that falls slightly as D increases. Both fits indicate that the luminosity in directed kinetic energy is independent of or very weakly dependent on the lobe-lobe separation D. This is consistent with the assumption adopted by Daly (1994), implicit in the relation between the total energy ejected by the compact object in the form of a highly collimated outflow $E_i \simeq L_j t_*$, that L_j is roughly constant over the source lifetime (see § 2.4 and Daly 1994).

The luminosity in directed kinetic energy is plotted as a function of redshift in Figure 2*b*; the line is the best-fit for galaxies only. There is no indication that the range or maximum value of the luminosity in directed kinetic energy increases strongly with redshift (though there may be a mild increase) for the radio galaxies out to a redshift of about 2.

Figure 2*c* illustrates the relation between the luminosity in directed kinetic energy L_j and the 178 MHz radio power P_r for galaxies. The parameters for the relation between L_j and the product of the radio power and the square root of the break frequency ν_b, $L_j(\sqrt{\nu_b} P_r)$, where both galaxies and quasars are included are listed in Table 2; nearly identical results are obtained when galaxies only are considered. The fits indicate that, roughly, $L_j \propto P_r^{0.75}$. The reduced χ^2 of the fit is rather large, but not quite as large as that seen in Figure 2*b*, and some of this scatter is probably due to departures of sources from equilibrium by different amounts, since the dependence of L_j on the magnetic field strength is rather strong. Note that $L_j \propto P_r^{0.75}$ is expected if the lobe radii and ambient gas density of different sources are similar (see Daly 1994, eq. [18a]).

If the strength of the magnetic field throughout the radio lobe is proportional to the average magnetic field strength of the entire radio-emitting region, then $L_j \propto \sqrt{\nu_b} P_r$. This follows since $L_j \propto v_L B^2 a_L^2$, where $B \propto (P_r/V)^{2/7}$, P_r is the total radio power, and V is the total volume of the radio-emitting region $V \propto a_L^2 D$, and the lobe propagation velocity $v_L \propto \sqrt{\nu_b} D B^{3/2}$, so $L_j \propto \sqrt{\nu_b} B^{7/2} D a_L^2 \propto \sqrt{\nu_b} P_r$. This is roughly consistent with the data, though the reduced χ^2 of the fit is rather large.

Figure 2*d* and Table 2 illustrate the dependence of L_j on the lobe propagation velocity v_L. It is interesting to note that for

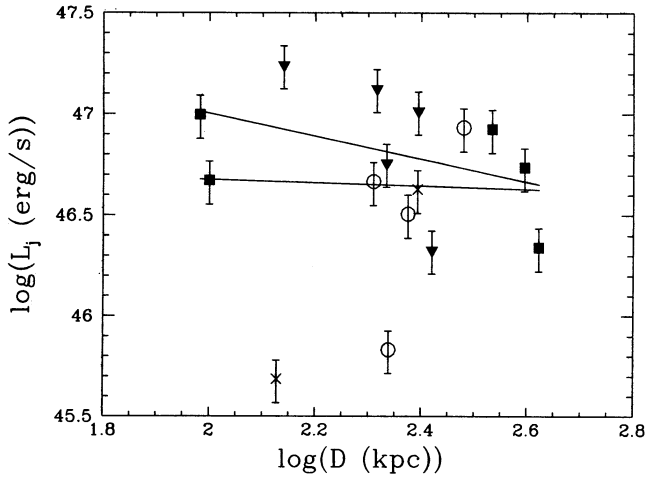

FIG. 2a

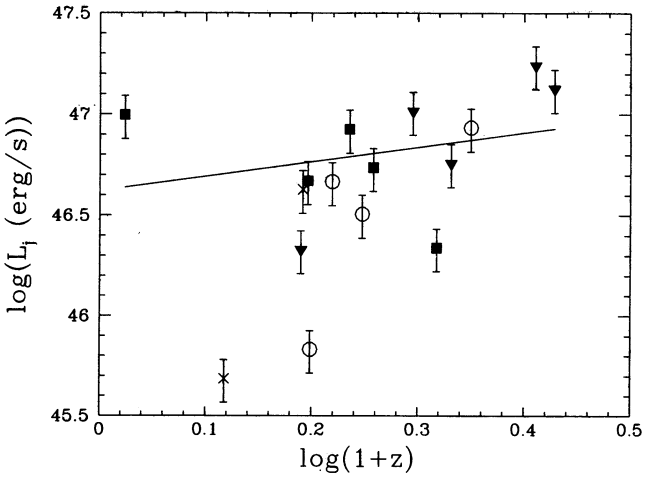

FIG. 2b

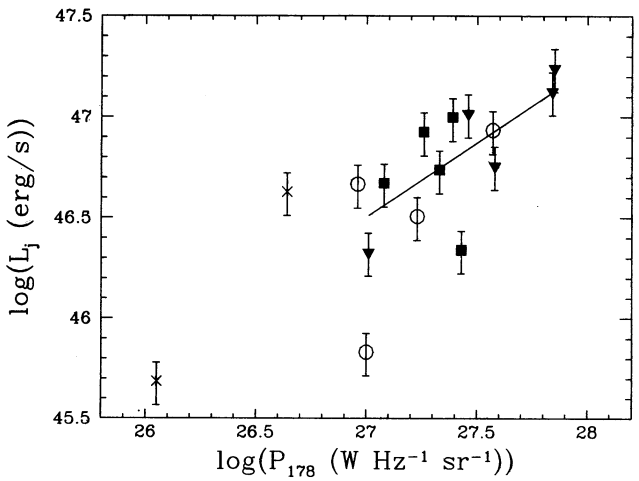

FIG. 2c

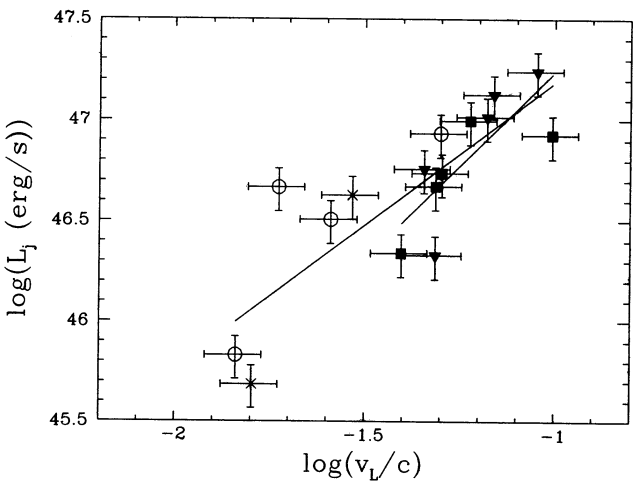

FIG. 2d

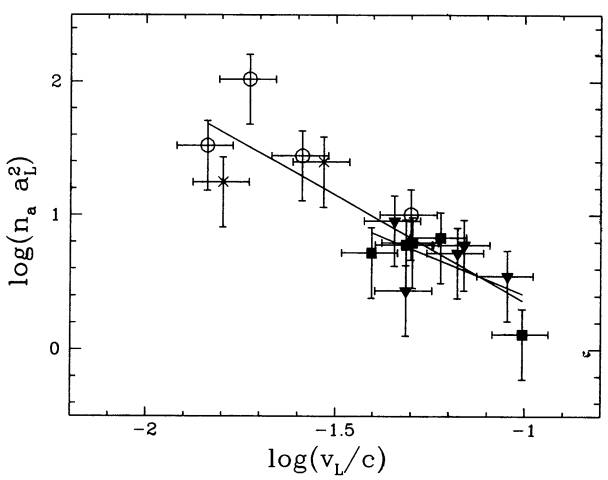

FIG. 2e

FIG. 2.—(*a–e*) Radio galaxies with resolved axial ratios are denoted by filled squares, and those with unresolved axial ratios, which result in a bound, are denoted by filled triangles, where the direction of the arrow indicates the direction of the bound. Quasars with 178 MHz powers between $h^{-2} \times (10^{26}$ and $10^{27})$ W Hz^{-1} sr^{-1} are denoted by crosses, while quasars with powers greater than $h^{-2} \times 10^{27}$ W Hz^{-1} sr^{-1} are denoted by open circles; all of the quasars have resolved axial ratios. Parameters of the best fitting lines are given in Table 2.

radio galaxies, the empirically determined relation is $L_j \propto v_L^2$, and for galaxies and quasars combined $L_j \propto v_L^{1.5}$, where L_j has been estimated using equation (3); $L_j \propto v_L^2$ is expected from the equation $L_j \propto v_h^2 A_h n_a v_j$ discussed in § 1 if $v_L \propto v_h$ with the other terms held roughly constant. The result that $L_j \propto v_L^2$ for radio galaxies suggests that $n_a a_L^2 \propto v_L^{-1}$ (see eq. [1]) for radio galaxies, which indeed is the case, as shown on Figure 2*e* and Table 2. Similarly, the result that $L_j \propto v_L^{1.5}$ for radio galaxies and quasars combined is completely consistent with the data since, for radio galaxies and quasars combined $n_a a_L^2 \propto v_L^{-1.5}$, as shown on Figure 2*e* and Table 2.

The parameter k that is important in the use of these sources as a calibrated yardstick is related to $n_a a_L^2$: $n_a a_L^2 = k^{-3}$ (see Daly 1994 and § 2.4), thus, the data imply that for radio galaxies $k \propto v_L^{1/3}$ and for quasars and galaxies combined $k \propto v_L^{1/2}$; the parameter k is discussed in § 2.4.

The dependence of v_L on $n_a a_L^2$ is listed in Table 2; it is interesting to consider the slope of this line since it is not clear whether to treat $n_a a_L^2$ or v_L as the independent variable for the fit. It is clear from Table 2 that the slopes obtained by interchanging the dependent and independent variables are inconsistent; this is possible because the best-fit line depends on the weights of the dependent variable only. However, the dependence of k, and thus $n_a a_L^2$, on v_L is quite important in using

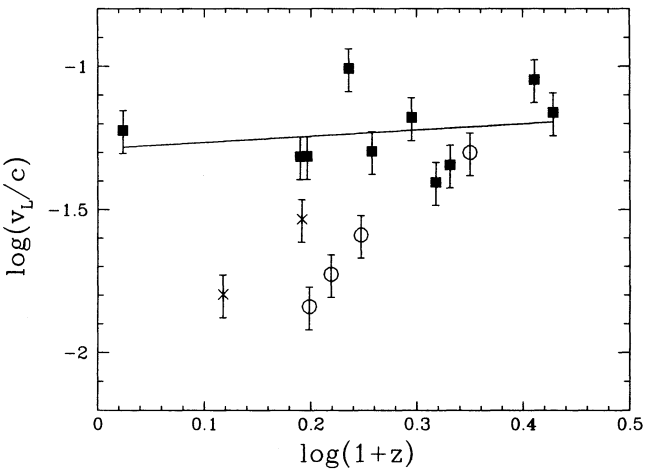

FIG. 3a

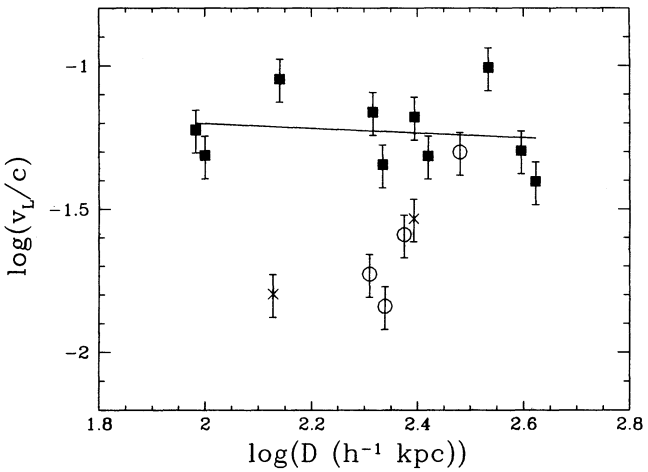

FIG. 3b

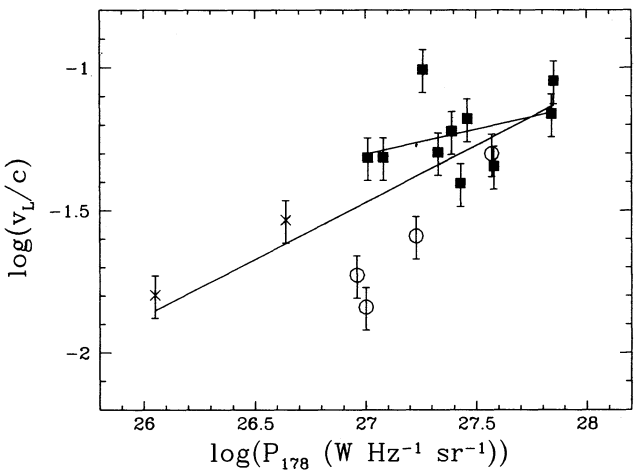

FIG. 3c

FIG. 3.—(*a–c*) Radio galaxies are denoted by filled squares. Quasars with 178 MHz powers between $h^{-2} \times (10^{26}$ and $10^{27})$ W Hz^{-1} sr^{-1} are denoted by crosses, while quasars with powers greater than $h^{-2} \times 10^{27}$ W Hz^{-1} sr^{-1} are denoted by open circles. Parameters of the best fitting lines are given in Table 2.

these sources for cosmology, as discussed in § 2.4 and by Daly (1994).

2.3. *Lobe Propagation Velocity*

The lobe propagation velocity for each source in the LMS89 data set was estimated by Daly (1994) and is listed in Table 1. LMS89 list the synchrotron age t of the source estimated across the radio-emitting region. Using a ruler, the fraction f_D of the lobe-lobe separation D, over which radio emission is detected, was measured. The lobe propagation velocity can then be estimated from $v_L = f_D D/(2t)$, where the lobes are assumed to propagate with equal velocity into the ambient medium and the average value of the two synchrotron ages was used, though in most cases the two values listed for t, one for each side of the radio bridge, are quite similar. In addition, the sources are fairly symmetric about the core region of the radio source. Using this method, the lobe propagation velocity of Cygnus A is estimated to be about $0.05c$ for $h = 1$, consistent with the results of Carilli et al. (1991).

The lobe propagation velocity as a function of redshift is shown in Figure 3*a*. The line indicates the best fit to the radio galaxies. The slope of the line is quite close to zero indicating little evolution of the lobe propagation velocity with redshift for the radio galaxies considered here. The reduced χ^2 of the fit is rather large, probably due to the different amounts by which different sources deviate from equipartition; note that $v_L \propto B^{1.5}$ when the dominant cooling mechanism is synchrotron cooling, as is assumed to be the case here (see Wellman & Daly 1995 for the effects of inverse Compton cooling). The observational uncertainties in estimating v_L amount to about 15% to 20%, so the large reduced χ^2 suggests that different deviations of the sources from minimum energy or equipartition conditions probably brings the total uncertainty to about 30%.

The relation between the lobe propagation velocity and the radio lobe separation is shown on Figure 3*b*; the line is the best-fit for radio galaxies. The slope of the line is zero indicating that the lobe propagation velocity is not strongly dependent on the lobe-lobe separation. This suggests that the approximation of constant lobe propagation velocity over the lifetime of a particular radio source, adopted by Daly (1994) in the use of these sources as a calibrated yardstick, is consistent with the data. The data may also imply a characteristic value for the lobe propagation velocity, at least for the radio galaxies. If the radio galaxies are in environments with similar sound speeds, such as would be expected if they are in clusters of galaxies with their intracluster media in place, then this implies a characteristic Mach number for the growth of the radio bridge as predicted by the numerical work of Lind et al. (1989).

Another interesting relation is that between the lobe propagation velocity and the radio power. Figure 3*c* and Table 2 show that when both galaxies and quasars are included in the fit, $v_L \propto P_r^{0.4}$, whereas when galaxies only are included in the fit $v_L \propto P_r^{0.2}$, though the two slopes are consistent at the 2 σ level. These results are consistent with those obtained by AL87 and LPR92; an explanation of this result has been put forward by Daly (1994, § 3.2). The difference between the $v_L(P_r)$ relations for galaxies compared with that for galaxies and quasars does suggest that this relation should be estimated for galaxies and quasars separately when the number of sources allow such estimates.

2.4. *Characteristic Source Sizes*

The characteristic source size l_*, introduced by Daly (1994), is approximately the average separation between the radio lobes that would be measured if the source could be observed for its entire lifetime t_*. For a constant v_L, this is half of the maximum lobe-lobe separation. The quantity l_* is time-independent for a given source, so the value of l_* estimated for a source should be the same, independent of when the source is observed in its evolution. The idea put forward by Daly (1994) is to estimate values of l_* for sources and compare this with the average values of lobe-lobe separations for a large sample of sources at similar redshifts. The calibrated yardstick l_* has a very different dependence on the cosmological model from the lobe-lobe separations, so their comparison can constrain the deceleration parameter q_0.

The characteristic source size l_* may be estimated by $l_* \simeq v_L t_*$ when the lobe propagation velocity is roughly constant over the lifetime of the radio source; t_* is the total or characteristic time for which the AGN produces a highly collimated outflow with luminosity in directed kinetic energy L_j. In this simple model, the source turns on, ejects a constant luminosity in directed kinetic energy L_j for a time t_*, and then switches off. Thus, the model assumes that both v_L and L_j are constant over the source lifetime. As discussed in § 2.3 and § 2.2, the data are consistent with v_L and L_j being roughly constant over the lifetime of a given source.

The AGN ejects a total energy E_i in the form of a luminosity in directed kinetic energy during the time t_*. If the energy source is the spin energy of a relatively isolated compact object, then the total energy ejected may be identified with the initial spin energy of the object, as would be the case for the model described by Wilson & Colbert (1995). The relation between the energy extraction rate L_j, the initial or total energy available to power the outflow E_i, and the characteristic time for which the outflow occurs t_*, is $t_* = E_i/L_j$, assuming that L_j is roughly constant over the lifetime of the source. The characteristic time for which the source is active may be written as a power law in L_j: $t_* \propto L_j^{-\beta/3}$ (Daly 1994). Such a parameterization allows one to account for many of the observed properties of powerful extended radio sources, as discussed in detail by Daly (1994).

Combining these expressions and using equations (1), (2), and (3), the characteristic source size is

$$l_* \propto k^{\beta} v_L^{1-\beta}, \tag{4}$$

where

$$k = \left(\frac{1}{n_a a_L^2}\right)^{1/3} \propto \left(\frac{v_L}{a_L B}\right)^{2/3}. \tag{5}$$

As discussed by Daly (1994), low-redshift observations suggest that the lobe-lobe separation of powerful extended radio sources is independent of v_L, and a host of other variables. Thus, if the dependence of k on v_L can be estimated, equation (4) can be used to estimate β, by choosing the value of β for which l_* is independent of v_L.

As discussed in § 2.2, it is not clear whether to treat k or v_L as the dependent variable to obtain the relation between k and v_L. Treating k as the dependent variable for galaxies indicates that $k \propto v_L^{1/3}$ for radio galaxies (see § 2.2); this would suggest that $\beta \sim 1.5$ for these sources. For the reasons discussed by Daly (1994), only radio galaxies provide a useful calibrated yardstick at this time.

Treating the lobe propagation velocity as the dependent variable, the best-fit line for the galaxies indicates that $v_L \propto (n_a a_L^2)^{-1/3}$ for galaxies, so $k \propto v_L$, which implies that $l_* \propto k^{\beta} v_L^{1-\beta}$ is independent of β, though this would imply that $l_* \propto v_L$, which is inconsistent with the data. The average value of the slopes for galaxies obtained here and above, treating v_L as the dependent and then the independent variable, indicates that $k \propto v_L^{2/3}$, which implies that $l_* \propto v_L^{1-\beta/3}$, suggesting a value of $\beta \sim 3$. The same slope is suggested by the combined galaxy and quasar data when the lobe propagation velocity is treated as the dependent variable (see Fig. 3*a* and Table 2); these data suggest $v_L \propto (n_a a_L^2)^{-0.5}$, so $k \propto v_L^{2/3}$ and $\beta \sim 3$ would imply that l_* is independent of the lobe propagation velocity v_L. These arguments suggest that β lies in the range from about 1.5 to 3. Other constraints on β are considered by Guerra & Daly (1995, 1996). Note that as β increases to values greater than 1, these sources become a more useful cosmological tool (Daly 1994).

The parameter k is plotted as a function of redshift in Figure 4*a*; the line indicated is fitted to the radio galaxies; k appears to be constant and independent of redshift at least out to a redshift of 1. Note that k is proportional to the axial ratio $R_T^{2/3}$, so only lower bounds on k exist for radio galaxies with redshifts greater than about 1.

It is interesting to note that the value of k for quasars is about half that for galaxies at a redshift of about 0.5. This is consistent with the results of Singal (1988) that the mean lobe-lobe separation of quasars is about half of that for galaxies at a redshift of about 0.5.

The parameter k is plotted as a function of lobe-lobe separation D in Figure 4*b*; the line is the fit to the radio galaxies. There is no indication that k depends on D. This shows that k is a characteristic source quantity and does not appear to vary strongly over the lifetime of the source.

As noted in § 2.3, the lobe propagation velocity is roughly independent of lobe-lobe separation and redshift. Since the characteristic source size depends on a combination of v_L and k (see eq. [4]), this means that the characteristic quantity l_* for the radio galaxies in the LMS89 data set is largely independent of redshift and lobe-lobe separation irrespective of the value of β.

The value of l_* is plotted as a function of redshift and lobe-lobe separation in Figures 4*c* and 4*d*, assuming a value of β of 1.5 and $q_0 = 0$. A comparison of the slopes of the lines and reduced χ^2 for Figures 4*a* and 4*c*, and for Figures 4*b* and 4*d* show that both $k(z)$ and $l_*(z)$, and $k(D)$ and $l_*(D)$ are consistent and yield similar fits to the radio galaxy data.

The form of l_* as a function of redshift should track the form of the average lobe-lobe separation for a large sample of sources, given that the correct cosmological model has been adopted; the average lobe-lobe separation for 3CR radio galaxies is shown by Kapahi (1989) for values of q_0 of 0 and 0.5. Figures 4*e* and 4*f* can be directly compared with these figures; Guerra & Daly (1995, 1996) are presently undertaking a quantitative comparison of these data sets. The log of l_* is plotted as a function of redshift in Figures 4*e* and 4*f* for values of β of 1.5 and 3, respectively. The parameters of the fit are listed in Table 2. Clearly, the characteristic source size appears to be constant from a redshift of 0 to a redshift of 1, and possibly to a redshift of 2, depending on whether the true axial ratios for the sources with unresolved axial ratios are close to the present bounds. The fact that the characteristic source sizes are constant at least to a redshift of 1, tends to favor an open universe, as

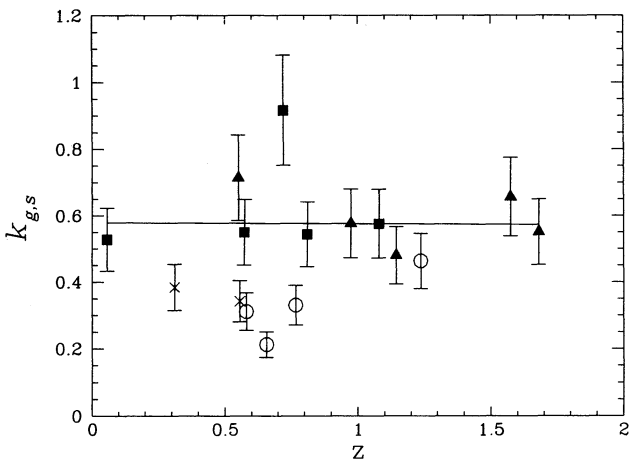

FIG. 4*a*

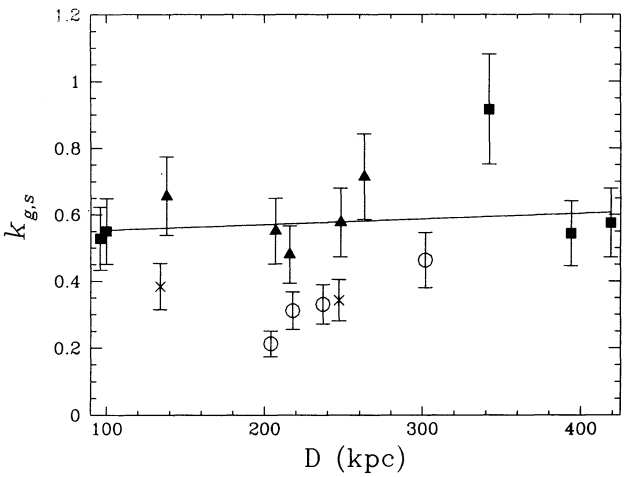

FIG. 4*b*

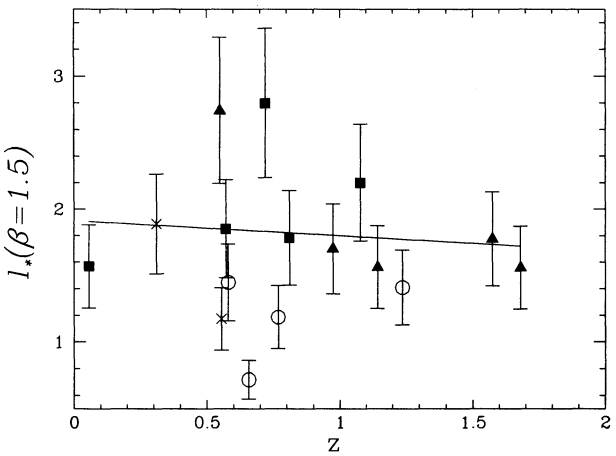

FIG. 4*c*

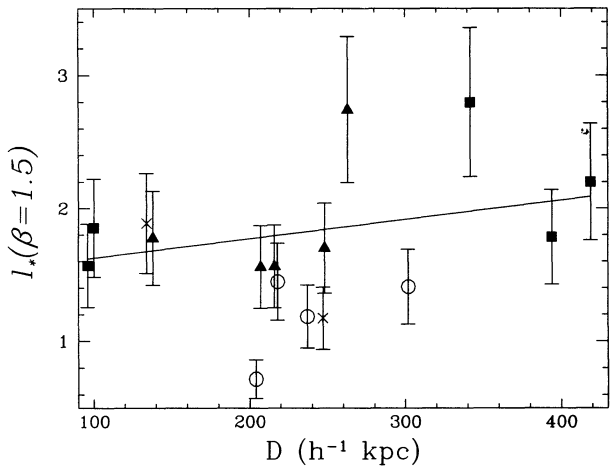

FIG. 4*d*

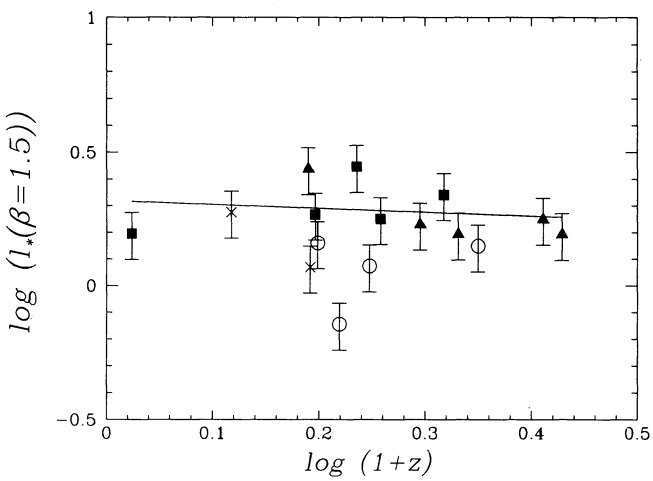

FIG. 4*e*

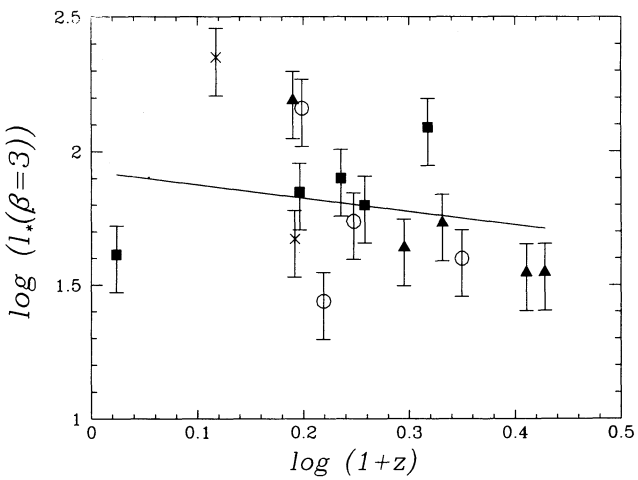

FIG. 4*f*

FIG. 4.—(*a–f*) Radio galaxies with resolved axial ratios are denoted by filled squares, and those with unresolved axial ratios, which result in a bound, are denoted by filled triangles, where the direction of the arrow indicates the direction of the bound. Quasars with 178 MHz powers between $h^{-2} \times (10^{26}$ and $10^{27})$ W Hz^{-1} sr^{-1} are denoted by crosses, while quasars with powers greater than $h^{-2} \times 10^{27}$ W Hz^{-1} sr^{-1} are denoted by open circles; all of the quasars have resolved axial ratios. Parameters of the best fitting lines are given in Table 2. (*g*) Radio galaxies are denoted by filled squares. Quasars with 178 MHz powers between $h^{-2} \times (10^{26}$ and $10^{27})$ W Hz^{-1} sr^{-1} are denoted by crosses, while quasars with powers greater than $h^{-2} \times 10^{27}$ W Hz^{-1} sr^{-1} are denoted by open circles.

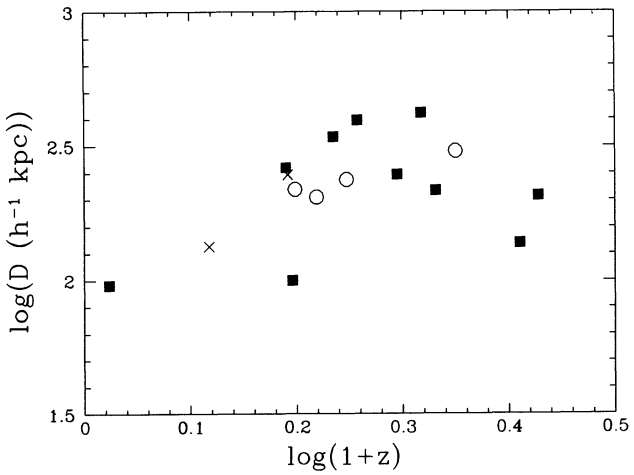

FIG. 4*g*

discussed by Daly (1994). However, given the present limited size of the data sets available, the work presented here is aimed more at demonstrating how the method can be applied to extract fundamental physical variables rather than at the specific world model indicated by the present analysis. For comparison, the lobe-lobe separations as a function of $(1 + z)$ for the sources used in the present analysis are presented in Figure 4*g*. A more detailed study, comparing the characteristic source sizes with the mean or median sizes estimated using a large sample of morphologically similar sources, is presently underway (Guerra & Daly 1995, 1996).

2.5. *Opening Angles, Lobe Radii, and Axial Ratios*

The opening angle, θ, may be estimated from $\tan \theta = a_L/(0.5D) = 1/R_T$, where R_T is the axial ratio of the source. The opening angle for the radio galaxies is much smaller than that for quasars, as illustrated on Figure 5*a* and as noted by LMS89. Note that the radio galaxies with lower bounds on axial ratios (*filled triangles*) have upper bounds on θ.

The lobe radii can be estimated from $a_L \simeq D/(2R)$ and are illustrated on Figure 5*b*. The lobe radii of the galaxies are typically much smaller than those of the quasars. The radio galaxies with lower bounds on axial ratios have upper bounds on their lobe radii.

The axial ratio of a source is approximately θ^{-1}. The parameters of the fit to $R_T(z)$ are listed in Table 2.

3. CONFRONTATION WITH ORIENTATION UNIFIED MODELS

Unified models of AGN attempt to fit the different types of AGN in the context of a single picture as discussed, for example, by Blandford (1987). A present favorite is the orientation unified model, in which radiation is emitted anisotropically from a central compact region and the AGN classification depends on the orientation of the observer relative to the anisotropic radiation field as discussed, for example, by Antonucci (1993). This picture is undoubtedly correct at some level and applies to some sources. However, it appears that the bridge widths of the radio galaxies are systematically smaller than those of radio-loud quasars (see § 2.5). LMS89 point out that the opening angles for quasars far exceed those for galaxies, though these authors note that this could be a selection effect. Further, Singal (1988) has shown that the redshift behavior of the median lobe-lobe sizes of radio galaxies is quite different from that of radio-loud quasars. And Daly (1992, § 7) points out that the velocity gradients across radio galaxies and radio-loud quasars follow a trend opposite to that expected in orientation unified models. Thus, there may be intrinsic differences between the different types of AGN, although orientation biases are also likely to play a role in observed differences.

Perhaps the two types of AGN activity should be directly linked to the two ultimate energy sources discussed for AGN, as discussed for example by Rees et al. (1982) and by Blandford (1992). The two ultimate energy sources widely discussed in the literature (e.g., Begelman, Blandford, & Rees 1984) are the spin energy of the central compact object and the gravitational binding energy of matter falling onto the central compact object. The two types of AGN activity observed are a highly collimated outflow, such as those that lead to powerful extended radio sources, and radiation emanating from a very

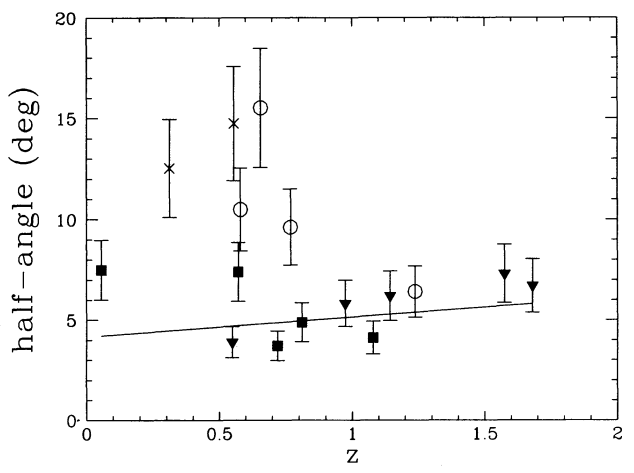

FIG. 5*a*

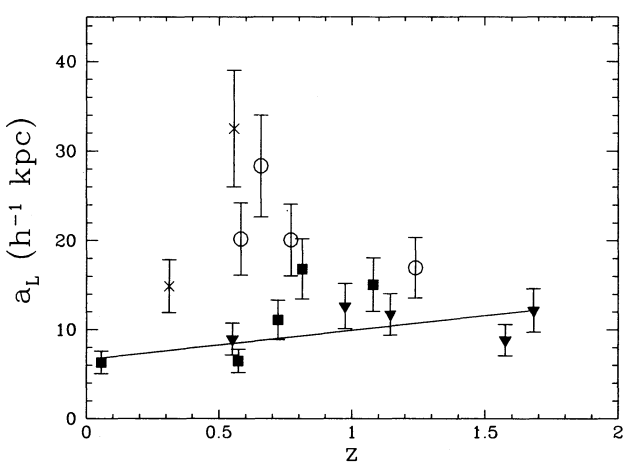

FIG. 5*b*

FIG. 5.—(*a*, *b*) Radio galaxies with resolved axial ratios are denoted by filled squares, and those with unresolved axial ratios, which result in a bound, are denoted by filled triangles, where the direction of the arrow indicates the direction of the bound. Quasars with 178 MHz powers between $h^{-2} \times (10^{26}$ and $10^{27})$ W Hz^{-1} sr^{-1} are denoted by crosses, while quasars with powers greater than $h^{-2} \times 10^{27}$ W Hz^{-1} sr^{-1} are denoted by open circles; all of the quasars have resolved axial ratios. Parameters of the best fitting lines are given in Table 2.

compact region. This suggests that the spin energy of the central compact source leads to highly collimated outflows, and the gravitational energy of matter falling onto the black hole leads to the radiant energy of the AGN.

This alternative view of AGN, discussed for example by Blandford (1992), is suggested by several facts including those presented in § 2.5, that both the lobe radii and opening angles are much larger for radio-loud quasars than they are for radio galaxies. Presumably, the extended radio emission is ultimately powered by a highly collimated outflow from the AGN in both cases. Suppose that an accretion disk, or other source of radiant energy near the central compact object, is present in the radio-loud quasars, but is much diminished in the radio galaxies, leading to their low radiant nonstellar luminosities. A massive magnetized accretion disk may cause the outflow to occur over a cone with a relatively large opening angle in the case of the radio-loud quasars, due to plasma interactions, for example, or due to the precession of the spin axis of the hole, but not in the case of the radio galaxies, since these would have a much diminished disk. Either of these effects could cause the opening angle and lobe radii of radio-loud quasars to be larger than those of radio galaxies, as observed.

Thus, the different properties of radio galaxies and radio-loud quasars could be understood if radio-loud quasars have a more massive or dynamically important accretion disk than radio galaxies. A more massive accretion disk would produce a more luminous source of radiation near the central compact object. Thus, the radiant nonstellar energy from the quasars would be much larger than that from the galaxies, which is consistent with the observations.

In this picture, the radio-loud quasars are powered by two separate energy reservoirs. The gravitational energy of matter falling onto the black hole powers the radiant luminosity that makes the source a quasar, and the spin energy of the compact object powers the highly collimated outflow. In radio galaxies, only the spin energy of the central compact source is being tapped. Radio-quiet quasars fit into this type of unification quite nicely; when energy from the gravitational infall of matter is available, but the spin energy of the compact source is not being tapped, the source is a radio-quiet quasar.

4. CONCLUSION

The way that the radio data can be used to estimate key physical parameters such as the ambient gas density and the luminosity in directed kinetic energy is demonstrated here. The strong shock jump conditions have been applied to the interface between the radio lobe and the ambient gas to estimate the ambient gas density in the vicinity of the radio lobe. At present, this appears to be the only method of estimating the ambient gas density (as a single parameter), and this first application of the method suggests that it works fairly well. This method has been used to estimate the ambient gas density in the vicinity of more high-redshift radio sources, and similar results are obtained (Wellman & Daly 1995, 1996).

The composite density profile obtained suggests that the powerful extended radio sources studied here are located in gaseous environments like those found in present-day clusters of galaxies, and that they lie in the cores of the clusters. This would imply that clusters of galaxies extending to at least 200 h^{-1} kpc, with their intracluster media in place, exist out to redshift of at least 1.7.

It is interesting to note that radio galaxies and radio-loud quasars are in very similar environments. The environments of these radio sources evolve weakly with redshift out to a redshift of about 2 (see § 2.1). It is likely that this is a selection effect; it may be that the AGN must lie in a relatively dense gaseous environment in order for the jet-medium interaction to produce a powerful radio source. However, it does imply that at least the central regions of some clusters of galaxies, with their intracluster media in place, exist at fairly large redshift. This is expected in models of structure formation and evolution in which structure formation is well under way at early epochs, as is expected in a low-density universe.

The rate at which energy is extracted from the central compact object and deposited near the radio hot spot is estimated and compared with other properties. The range and upper envelope of the energy extraction rate do not appear to depend strongly on redshift for the radio galaxies, and there are too few radio-loud quasars to investigate whether this is true of the quasars. The maximum energy extraction rate appears to be comparable to that of Cygnus A.

The velocity of lobe propagation for the radio galaxies seems to exhibit a maximum value and a characteristic value. If the sources are in environments with similar sound speeds, such as the intracluster media in clusters of galaxies, this would indicate that they have a typical Mach number. This is consistent with theoretical expectations based on numerical simulations (Lind et al. 1989).

The time-independent characteristic source sizes are analyzed and discussed. The model presented by Daly (1994) and applied as a cosmological tool has been subject to a variety of tests to check the internal consistency of the model. There are no obvious internal inconsistencies. For example, the data are consistent with the assumptions (needed for the use of the sources as a cosmological tool, but not for the estimates of the ambient gas density and luminosity in directed kinetic energy) that the energy extraction rate L_j of a given source is time-independent over the lifetime of the source, and the lobe propagation velocity of a given source is roughly constant over the source lifetime. The data for the radio galaxies indicate that the upper envelope and range of luminosities in directed kinetic energy do not evolve with redshift, suggesting that relations between the energy extraction rate L_j and the characteristic source lifetime t_* fixed at low redshift may be applied to high-redshift sources.

A comparison of the radio properties of radio-loud quasars and radio galaxies suggests yet another view of the three types of AGN observed. The types of AGN activity observed are separated into highly collimated outflows, such as those that power extended radio emission, and nonstellar radiant emission arising from the nuclear region of the source. This supports the ideas discussed for example by Rees et al. (1982) and by Blandford (1992). Perhaps the two types of activity are associated with the two energy sources that are ultimately available from a compact object: the gravitational energy of matter falling onto the black hole powers the radiant nuclear luminosity of the AGN and produces "quasars," and the tapping of the spin energy powers the luminosity in directed kinetic energy or the highly collimated outflow and produces jets and radio sources. Then, radio galaxies result when the spin energy is being tapped, radio-loud quasars result when both the spin energy and the gravitational binding energy are being tapped, and radio-quiet quasars result when the gravitational binding energy is being tapped.

Clearly, powerful extended radio sources provide an invaluable probe of a rich variety of interesting physical variables

and of the evolution of the gaseous environments of the sources.

It is a pleasure to thank Roger Blandford, Dave De Young, George Field, Ed Groth, Eddie Guerra, Paddy Leahy, Alan Marscher, Jerry Ostriker, Lyman Page, Jim Peebles, Rick Perley, Martin Rees, Larry Rudnick, Richard Saunders, Hy Spinrad, Greg Wellman, Lin Wan and Dave Wilkinson for helpful discussions. I would also like to thank an anonymous referee for several helpful comments that substantially improved the paper. This work was supported in part by the US National Science Foundation.

REFERENCES

Alexander, P., & Leahy, J. P. 1987, MNRAS, 225, 1 (AL87)
Antonucci, R. 1993, ARA&A, 31, 473
Arnaud, K. A., Fabian, A. C., Eales, S. A., Jones, C., & Forman, W. 1984, MNRAS, 211, 981
Begelman, M. C., Blandford, R. D., & Rees, M. J. 1984, Rev. Mod. Phys., 56, 255
Begelman, M. C., & Cioffi, D. 1989, ApJ, 345, L21
Black, A. R. S., Baum, S. A., Leahy, J. P., Perley, R. A., Riley, J. M., & Scheuer, P. A. G. 1992, MNRAS, 256, 186
Blandford, R. D. 1992, in Physics of Active Galactic Nuclei, ed. W. J. Duschl & S. J. Wagner (Berlin: Springer), 3
———. 1987, in Superluminal Radio Sources, ed. J. A. Zensus & T. J. Pearson (Cambridge: Cambridge Univ. Press), 310
Blandford, R. D., & Rees, M. J. 1974, MNRAS, 169, 395
Bridle, A. H., & Perley, R. A. 1984, ARA&A, 22, 319
Carilli, C. L., Perley, R. A., Dreher, J. W., & Leahy, J. P. 1991, ApJ, 383, 554
Chevalier, R. A., & Imamura, J. N. 1983, ApJ, 270, 554
Cox, C. I., Gull, S. F., & Scheuer, P. A. G. 1991, MNRAS, 252, 558
Daly, R. A. 1990, ApJ, 355, 416
———. 1992, ApJ, 399, 426
———. 1993, ApJ, 406, 47
———. 1994, ApJ, 426, 38
De Young, D. S. 1971, ApJ, 167, 541
———. 1986, ApJ, 307, 62
———. 1991, ApJ, 371, 69
De Young, D. S., & Axford, W. I. 1967, Nature, 216, 129
Guerra, E., & Daly, R. A. 1995, ApJ, submitted
———. 1996, in Cygnus A Workshop, ed. C. Carilli & D. Harris (Cambridge: Cambridge Univ. Press), in press
Hundhausen, A. J. 1985, in Collisionless Shocks in the Heliosphere: A Tutorial Review, ed. R. G. Stone & B. T. Tsurwtaui (Washington, DC: Am. Geophys. Union), 37
Jones, C., & Forman, W. 1984, ApJ, 276, 38
Kapahi, V. K. 1987, in Observational Cosmology, ed. A. Hewitt, G. Burbidge, & L. Z. Fang (Dordrecht: Reidel), 251
———. 1989, AJ, 97, 1
Lacy, M., Hill, G. J., Kaiser, M., & Rawlings, S. 1993, MNRAS, 263, 707
Leahy, J. P. 1991, in Beams and Jets in Astrophysics, ed. P. A. Hughes (Cambridge: Cambridge Univ. Press), 100
Leahy, J. P., Muxlow, T. W. B., & Stephens, P. W. 1989, MNRAS, 239, 401 (LMS89)
Leahy, J. P., & Williams, A. G. 1984, MNRAS, 210, 929
Lind, K. R., Payne, D. G., Meier, D. L., & Blandford, R. D. 1989, ApJ, 344, 89
Liu, R., Pooley, G., & Riley, J. M. 1992, MNRAS, 257, 545 (LPR92)
Loken, C., Burns, J. O., Clarke, D. A., & Norman, M. L. 1992, ApJ, 392, 54
McKee, C. F., & Ostriker, J. P. 1977, ApJ, 218, 148
Myers, S. T., & Spangler, S. R. 1985, ApJ, 291, 52
Norman, M. L., Smarr, L., Winkler, K.-H. A., & Smith, M. D. 1982, A&A, 113, 285
Parker, E. N. 1963, Interplanetary Dynamical Processes (New York: Interscience)
Prestage, R. M., & Peacock, J. A. 1988, MNRAS, 230, 131
Rawlings, S., & Saunders, R. 1991, Nature, 349, 138
Rees, M. J. 1989, MNRAS, 239, 1P
Rees, M. J., Begelman, M. C., Blandford, R. D., & Phinney, E. S. 1982, Nature, 295, 17
Scheuer, P. A. G. 1974, MNRAS, 166, 513
———. 1982, in IAU Symp. 97, Extragalactic Radio Sources, ed. D. S. Heeschen & C. M. Wade (Dordrecht: Reidel), 163
Singal, A. K. 1988, MNRAS, 233, 87
Wellman, G., & Daly, R. A. 1995, ApJ, submitted
———. 1996, in Cygnus A Workshop, ed. C. Carilli & D. Harris (Cambridge: Cambridge Univ. Press), in press
Wilson, A. S., & Colbert, E. J. M. 1995, ApJ, 438, 62